Andrew R. Casey, Stefan Keller and Gary Da Costa
Research School of Astronomy & Astrophysics, Australian National University, Canberra, Australia

ABSTRACT

We present observations obtained with the AAT's 2dF wide field spectrograph AAOmega of 3,453 K-type stars. These stars are located within the Virgo Over-Density and along the leading arm of the Sagittarius Stream. Through comparisons with N-body models of the Galaxy-Sagittarius interaction, we find a tri-axial dark matter halo is favoured and we preclude a prolate shape. This result is contradictory with other observations along the Sagittarius leading arm, which typically favour prolate models. We have also uncovered K-giant members of Sagittarius which are notably more metal poor ($\langle$[Fe/H]$\rangle = -1.73 \pm 0.33$) than previous studies. This suggests a significantly wider metallicity distribution exists in the Sagittarius stream than formerly considered.

Subject headings: Galaxy: halo, structure — Individual: Sagittarius, Virgo Stellar Stream — Stars: K-giants

1. Introduction

The proportion of substructure recently uncovered in the Galaxy has highlighted the crucial involvement accretion has played in the formation of the Milky Way. Properties of these stellar structures allow us to probe the formation mechanisms and history of the Galaxy. Recent studies (Carollo et al. 2007, 2010) have suggested multiple evolution methods are required for galaxy formation to reconcile observational evidence, although this is a subject of ongoing debate (Schoenrich et al. 2010). Regardless, the dissipation-less merging paradigm is widely accepted, and consistent with favoured Cold Dark Matter (ΛCDM) cosmology models. Through the examination of ongoing accretion events in the Milky Way and fossils from previous mergers, we can ultimately trace the formation history of the Galaxy.

Accretion is at least partly (Starkenburg et al. 2009), if not entirely responsible for the formation of the stellar halo. Bell et al. (2008) compared Sloan Digital Sky Survey (York et al. 2000, hereafter SDSS) data to galaxy formation simulations using different dark halos and found that observations are consistent with the stellar halo being entirely formed by hierarchical merging of accreted satellites (see also Xue et al. (2010)).

Unquestionably the most prominent accretion event within the Milky Way is that of the Sagittarius (Sgr) dwarf Spheroidal (dSph) galaxy. Originally uncovered by Ibata et al. (1994) as a comoving group of K- and M-type giants, the tidal tails of Sgr circle our Galaxy. As such they have been extensively traced with red-clump stars (Majewski et al. 1999), carbon stars (Totten & Irwin 1998; Ibata et al. 2001), RR Lyrae stars (Ivezić et al. 2000; Vivas et al. 2005; Keller et al. 2008; Watkins et al. 2009; Prior et al. 2009b), A-type stars (Newberg et al. 2003) and K/M-giants (Majewski et al. 2003). With spatial and kinematical information, tracers originating from the dwarf host can be unequivocally identified. This is because they remain dynamically cold, and are identifiable as kinematic substructures long after they are stripped from their progenitor (for example Ibata & Lewis 1998; Helmi & White 1999).

Stellar tracers within these tails are kinematically sensitive to the galactic potential. This has led various groups to model the Sgr interaction with different dark matter profiles. Martínez-Delgado et al. (2004) traced the Northern arm and found a near spherical or oblate ($q \approx 0.85$) dark matter halo best represented the observed debris, which coincided with the findings of Ibata et al.

(2001). In contrast Helmi (2004) found evidence in the Sgr leading debris that most favoured a prolate ($q = 1.25$) halo. Vivas et al. (2005) found that either a prolate or spherical model of Helmi (2004) would fit their observed RR Lyrae data, rather than those of an oblate model. Johnston et al. (2005) later pointed out that no prolate model can reproduce the orbital pole precession of the Sgr debris, but an oblate potential could. Law et al. (2005, hereafter LJM05) performed simulations using data of the Sgr debris from the 2-Micron All Sky Survey (2MASS) catalogue and found that the kinematics of leading debris was best fit by prolate halos, whereas the trailing debris typically favoured oblate halos.

Belokurov et al. (2006) found an apparent bifurcation within the Sgr debris, which Fellhauer et al. (2006) argued can only result from a dark halo having a near spherical shape. Law et al. (2009) introduced a tri-axial model with a varying flattening profile q, which replicates the orbital precession seen and matched kinematic observations of the Sgr debris. However Law & Majewski (2010) (hereafter LM10) conceded this may be a purely numerical solution as tri-axial halos are dynamically unstable, and admits more kinematic measurements in other regions of the Sgr stream are required.

After the Sgr stellar stream, the Virgo Over-Density (VOD) is arguably the next most significant substructure within our Galaxy. The first over-density in the vicinity of the VOD was observed as a group of RR Lyrae stars by the QUEST survey (Vivas et al. 2001). The collaboration later named this the "$12^{\rm h}.4$ clump" (Zinn et al. 2004). The broad nature of the VOD was later uncovered from the SDSS catalogue as a diffuse over-density of main-sequence turnoff stars centered at $r_\odot \sim 18$ kpc (which Newberg et al. 2002, dubbed as S297+63-20.5). The nomenclature on the substructure names within this region is varied, however when referring to the VOD we are discussing the spatial over-density of stars within the region, separate from any co-moving groups.

The difficulty arises in accurately distinguishing the VOD. There are multiple substructures along this line of sight. Duffau et al. (2006) took observations of BHB and RR Lyrae within the "$12^{\rm h}.4$ clump" and found a common velocity of $V_{GSR} = 99.8$ km s^{-1} with $\sigma = 17.3$ km s^{-1}. The dispersion in kinematics measured by Duffau et al. (2006) is essentially the velocity precision, so the substructure may possess a much smaller σ_v. This co-moving group was coined the Virgo Stellar Stream (VSS) and thus differentiated it from the broad spatial over-density. This distinction from the VOD was somewhat strengthened with new distance measurements which placed the VOD centroid at $r_\odot = 16$ kpc (Jurić et al. 2008; Keller 2010), and the VSS 3 kpc further away (Duffau et al. 2006). Although when considered in the light of systematic and observational uncertainties, this is of marginal significance. Moreover Jurić et al. (2008) suggests the VOD may extend between $r_\odot = 6$ to 20 kpc, which further complicates the matter of distance separation.

The relationship between the VSS and the S297+63-20.5 over-density is still unclear. Newberg et al. (2007) found a kinematic signature of $V_{GSR} = 130 \pm 10$ km s^{-1} for members of the VOD/S297+63-20.5, which is extremely close to the VSS peak. The VSS and S297+63-20.5 are co-incident in space, but their velocity difference has not yet been reconciled. The distance measurements between S297+63-20.5 and the VSS are similar enough ($\sim$ 1 kpc) within probable distance uncertainties for Newberg et al. (2007) and Prior et al. (2009b) to infer they are part of the same structure. Newberg et al. (2007) estimate a distance to S297+63-20.5 of $r_\odot = 18$ kpc from $g_0 = 20.5$ turnoff stars, but they concede the structure is likely dispersed along the line of sight as the Color-Magnitude Diagram (CMD) for this region does not demonstrate a tight sequence. Certainly this region of sky, aptly coined the 'Field of Streams' by Belokurov et al. (2006) is complex territory.

Photometric studies are inadequate to fully untangle this region. Kinematics are essential to identify co-moving groups which are distinct from the halo. Chemical information is vital to accurately distinguish these substructures and understand their origins. However, very few studies have directly investigated metallicities for these stars. In this paper we present spectroscopic observations of K-giants in this region. Substructure kinematics are used to probe the shape of dark matter in the Galaxy. We report both the velocities and metallicities of these giants in an effort to help untangle this accreted-dominated region.

Target selection methodology is outlined in the next section, which is followed with details regarding the observations. Techniques used to separate K-giants from dwarfs are discussed in §4, and our analysis procedure for kinematics (§5) and metallicities (§6) follows. A discussion of substructures is outlined in §7 and in §9 we conclude with some final remarks and critical interpretations.

2. Target Selection

When the presence of a stellar substructure is uncovered K-giants provide excellent candidates for spectroscopic follow-up. They allow for precise radial velocities and chemical abundances. In order to specifically target K-giants, we have chosen candidates within the colour selection box shown in Figure 1, taken from the SDSS DR7 catalogue. Field dwarfs are expected to contaminate the sample due to their similarity in colours. Although K-dwarfs are difficult to distinguish photometrically, we can spectroscopically separate these through the equivalent width (EW) of the gravity-sensitive triplet Mg I lines at 5167.3, 5172.7, and 5183.6 Å (see §4).

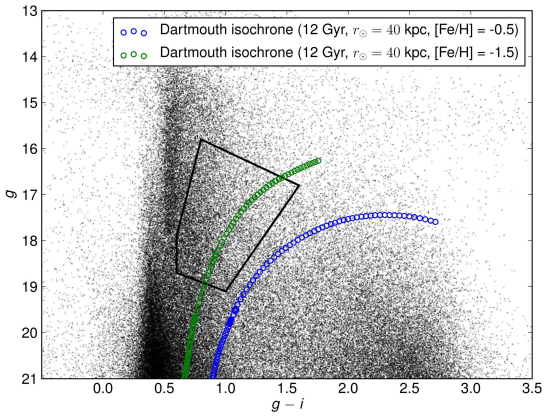

Fig. 1.— CMD of our observed regions from SDSS DR7, overlaid with the colour selection criterion used to target K-giants. Appropriate Dartmouth isochrones (Dotter et al. 2008) are shown for Sgr debris at a distance of $r_\odot = 40$ kpc (Belokurov et al. 2006)

3. Observations

Our targets were observed over two runs using AAOmega on the 3.9-m Anglo-Australian Telescope (now the Australian Astronomical Telescope) at Siding Springs Observatory in New South Wales, Australia. AAOmega is a double-beam, multi-object fibre-fed spectrograph covering a two degree field of view. The targets were observed in normal visitor mode in April 2009. Throughout all observations, sufficient sky and guide fibres ($\sim$ 30 and 7-8 respectively) were allocated to ensure optimal sky subtraction and astrometry. In total 3,453 science targets were observed across 4 fields (Table 1). Multiple configurations were observed for most fields to permit measurements of bright ($g < 16$) and faint ($g > 16$) stars, as well as repeat observations on a subset of stars.

The beam was split into the red and blue arms using the 5700 Å dichroic. The 580V grating in the blue arm yields spectra between 370-580 nm, with a resolution of $R = 1300$. In the red arm we used the 1000I grating which spans the spectral range from 800-950 nm. This coverage includes the Ca II NIR Triplet (CaT), which is used for radial velocities and metallicities. To minimise scattered-light cross talk between fibres, science targets on each configuration were limited to 1.5 magnitudes in range. Globular clusters NGC 5024, 5053 and 5904 were observed as radial velocity and metallicity standards.

The data was reduced using the 2DFDR[1] pipeline. After being flat-fielded, the fibres were throughput calibrated and the sky spectrum was subtracted using the median of the dedicated sky fibres. Wavelength calibration was achieved from arc lamp exposures taken between each set of science fields. Multiple object frames were successively taken to assist with cosmic ray removal. Three thirty-minute science exposures were taken for each faint field, and three twenty-five minute exposures for bright fields.

4. Dwarf / Giant separation

When discussing our data with respect to stellar streams and substructures within the halo, we are referring only to K-type giants. Dwarfs that fall

[1] http://www.aao.gov.au/AAO/2df/aaomega

Table 1
Observed fields

Field	α-center (J2000.0)	δ-center (J2000.0)	Plate Targets
A	12 00 00	+00 00 00	1
B	12 20 00	−01 00 00	2
C	12 40 00	−02 00 00	3
D	12 56 00	−02 42 00	6

within our apparent magnitude limit are not sufficiently distant to probe halo substructures. Our resolution is adequate such that the Mg I triplet lines can be individually measured and used to discriminate dwarfs.

A grid of synthetic spectra has been generated to quantitively establish a giant/dwarf separation criterion. The grid was generated using Castelli & Kurucz (2004) model atmospheres with MOOG[2] and the line list of Kurucz & Bell (1995). Spectra was also generated using stellar parameters for the Sun and Arcturus. The strength of the Mg I lines were tuned to match both the Solar and Arcturus atlases of Hinkle et al. (2003). Girardi et al. (2004) isochrones have been used to translate our observed $g-i$ colour range to effective temperature. This corresponds to a temperature range for our grid from 3900 to 5200 K, stepped at 25 K intervals. We have assumed typical K-type surface gravities of $\log g = 2$ for giants and $\log g = 4.5$ for dwarfs. Metallicities of [Fe/H] $= -0.5$, -1.5, and -2.5 were considered for both surface gravities.

All synthetic spectra was mapped onto the same wavelength space as our observations. Intensity was convolved with a Gaussian kernel of 3.03 Å to match our observed resolution. Mg I line strengths for our observations and synthetic spectra is shown against $g-i$ in Figure 2. As expected, there is an overlap of Mg I strengths between metal-rich "giants" ($\log g = 2$) and metal-poor "dwarfs" ($\log g = 4.5$). However, we do not expect metal-poor dwarfs to be a principle contaminant due to their intrinsically low luminosities and paucity. Using our synthetic grid, we have varied the slope and offset of our separation line to assess the effectiveness in differentiating giants from dwarfs. A linear rule has been adopted to differentiate the populations, which maximises giant

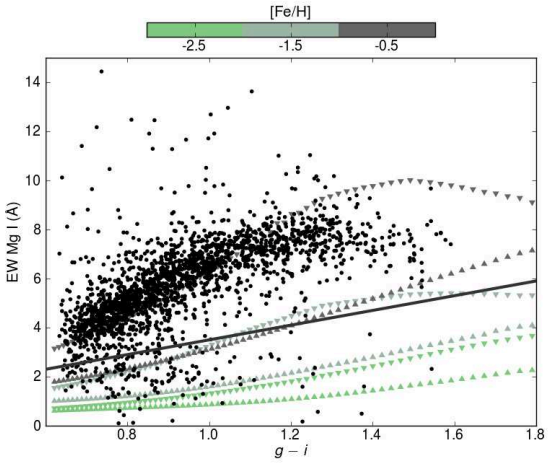

Fig. 2.— The sum of the Mg I triplet EWs for observations and synthetic spectra shown against the Sloan $g-i$ colour. Synthetic spectra is shown for $\log g = 2$ ($\triangle$) and $\log g = 4.5$ ($\triangledown$), and points are coloured by metallicity. Our dwarf/giant separation line is shown (solid).

recoverability with minimal contamination. Using the rule,

$$EW_{Mg\,I} < 3(g-i) + 0.5 \qquad (1)$$

we identify 185 giants in our observed fields. An analysis of our 185 giant candidates revealed three stars with high proper motions, all of which lay close to our dwarf/giant separation line. This suggests they are dwarfs, and have been excluded. Some possible giant targets were discarded due to insufficient S/N, or because the Mg I triplet fell on faulty regions of the detector. All efforts were made to minimise these losses. The distilled giant sample size is 178.

[2]http://www.as.utexas.edu/~chris/moog.html

5. Radial Velocities

The Ca II triplet absorption lines at 8498.0, 8542.1 and 8662.1 Å have been used to measure radial velocities. These lines are strong, and easily identifiable in Red Giant Branch (RGB) stars even at low resolution. Observed spectra have been cross-correlated with typical synthetic spectra of a K-giant ($T_{eff} = 4500$ K, $\log g = 2$, [Fe/H] $= -1.5$), and heliocentric corrections were made. Radial velocity measurements made on the standard stars in our globular clusters agree (within 3 km s^{-1}) with the catalogue of Harris (1996) (2011 edition). A number of our targets were observed on multiple fields, which allows us to calculate the internal measurement error. The differences between multiple measurements of the same target was calculated, and they form a half-normal distribution with a HWHM = 3.58 km s^{-1} .This measurement includes velocity measurements of identified dwarfs, as we are focussed here on determining the systematic accuracy of our velocity measurements and not identifying substructures.

In order to compare our kinematic results in a homogenous manner, we have translated our heliocentric velocities to a galactocentric frame. We have adopted the circular velocity of the Local Standard of Rest (LSR) at the Sun as 220 km s^{-1} (Kerr & Lynden-Bell 1986) and accounted for the Sun's peculiar velocity to the LSR by using 16.5 km s^{-1} towards $l = 53°, b = 25°$ (Mihalas & Binney 1981). The corrected line of sight velocity is then given by,

$$\begin{aligned} V_{GSR} = \; & V_{OBS} + 220 \sin l \cos b + 16.5 \qquad (2) \\ & \times [\sin b \sin 25 + \cos b \cos 25 \cos (l - 53)] \end{aligned}$$

where V_{OBS} is the heliocentric corrected observed line of sight velocity. A caveat to this reference transformation is that other authors in the literature have used slightly different formulae to transpose their kinematics to a galactocentric frame. This will result in a systematic shift in velocities between authors. Impacts from this variation are discussed later in the text.

6. Metallicities

We have ascertained metallicities for our giants using the strength of the Ca triplet lines. This technique was originally empirically described for individual stars in globular clusters (Armandroff & Da Costa 1991). A spectroscopic analysis using VLT/FLAMES observations of RGB stars from composite populations led Battaglia et al. (2008) to conclude that a calibrated CaT-[Fe/H] relationship can be confidently used in composite stellar populations (see also Rutledge et al. 1997; Starkenburg et al. 2010). The caveat to this technique is that a luminosity (specifically $V - V_{HB}$) is required for calibration, and we have to assume a V_{HB} luminosity here. Johnson V-band magnitudes were calculated from SDSS *ugriz* photometry using Jester et al. (2005) transformations. The weaker third Ca triplet line is more susceptible to noise and residual sky-line contamination (Tolstoy et al. 2001; Battaglia et al. 2008). Consequently, the strongest two CaT lines (8542 and 8662λ) have been used to form a reduced EW (W') such that,

$$\begin{aligned} \textstyle\sum W &= EW_{8542} + EW_{8662} \qquad (3) \\ W' &= \textstyle\sum W + 0.64\,(\pm 0.02)\,(V - V_{HB}) \qquad (4) \end{aligned}$$

and the metallicity linearly varies with W' where,

$$[\mathrm{Fe/H}]_{\mathrm{CaT}} = (-2.81 \pm 0.16) + (0.44 \pm 0.04) W' \quad (5)$$

Using this calibration, our globular cluster standard stars (with known V_{HB} magnitudes) have metallicities that match well with the Harris (1996) catalogue (2011 edition). Only K-giants within the valid calibration range ($0 > V - V_{HB} > -3$) were considered for metallicities. We assume that we have two dominant substructures present in our observations; the leading arm of Sagittarius and the Virgo Over-Density (see §7.1). The Sagittarius stream dominates our negative V_{GSR} population, and our positive kinematic space is primarily comprised of VOD members. As such we have separated our population at $V_{GSR} = 0$ into two samples with assumed V_{HB} magnitudes. Although this introduces a (known) systemic effect, it is a required assumption to estimate the metallicity distribution of each population.

The horizontal branch magnitude assumed for the VSS/VOD has been ascertained from previous RR Lyrae studies. As RR Lyraes sit on the horizontal branch, the V_{HB} is taken as the V-band median of four Prior et al. (2009b) and three Duffau et al. (2006) VSS members to yield $\langle V \rangle = 17.09$. This combined value precisely matches the mean solely reported by Duffau et al. (2006). In our

K-giant sample with positive galactocentric velocities, we assume $V_{HB} = 17.09$ which implies these stars are at a distance of ~ 20 kpc.

As the distance to the Sgr debris varies greatly throughout the halo, the horizontal branch magnitude varies with the position along the stream. Through CMD comparisons with the Sgr core (Bellazzini et al. 2006), Belokurov et al. (2006) determined distances along the two branches of the Sgr bifurcation. Revised distance measurements by Siegel et al. (2007) (as tabulated in Table 1 of LM10) have been crucial in constraining dark halo models. Our observations lay on the edge of Branch A (Figure 5).

We have assumed distances to these stars by interpolating their position along a cubic spline fitted to published distances. The horizontal branch magnitude V_{HB} is calculated using this assumed distance and the known luminosity of RR Lyrae stars ($M_V = +0.69$; Tsujimoto et al. 1998). Reddening is accounted for using the Schlegel et al. (1998) maps. Uncertainties in distance are not interpolated; they are taken as the largest published uncertainty of the closest neighbouring data points, and this is propagated through to our reported metallicity uncertainties.

7. Discussion

7.1. Substructure Identification

A significant kinematic deviation from a canonical halo population signifies a co-moving group. There are multiple substructures along our line-of-sight. These features are identified first and discussed separately. We have represented our galactocentric velocities with a generalised histogram (Figure 3) to quantitatively compare the kinematics of stars in our sample to a representative halo distribution.

The generalised histogram represents each data point with a Gaussian kernel of an equal bandwidth (deviation). As our internal kinematic errors between multiple measurements summate to a half-normal distribution with a FWHM of 7.16 km s^{-1}, we have opted for a bandwidth value of 10 km s^{-1} the generalised histogram in Figure 3 to avoid under-smoothing.

The most significant ($> 3\sigma$) kinematic peaks have been labeled Features A, B, and C. Features

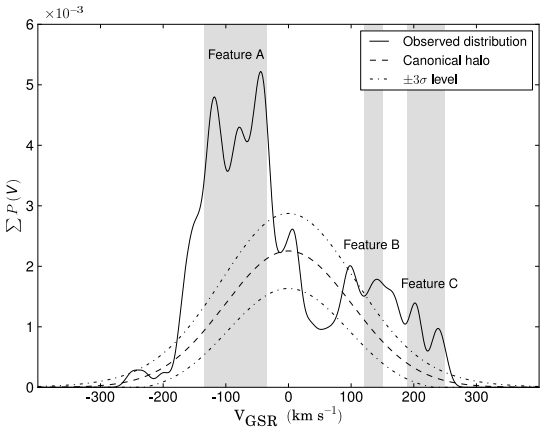

Fig. 3.— Generalised histogram of V_{GSR} for our 178 K-type giants, highlighting their significance against a canonical halo population with $\mu = 0$ km s^{-1}, $\sigma = 101.6$ km s^{-1} (Sirko et al. 2004). The Gaussian is normalised such that the integral equals the number of observed stars excluding those outside a 2.5-σ excess. Significant ($> 3\sigma$) kinematic deviations from the smooth distribution are appropriately grouped and labelled.

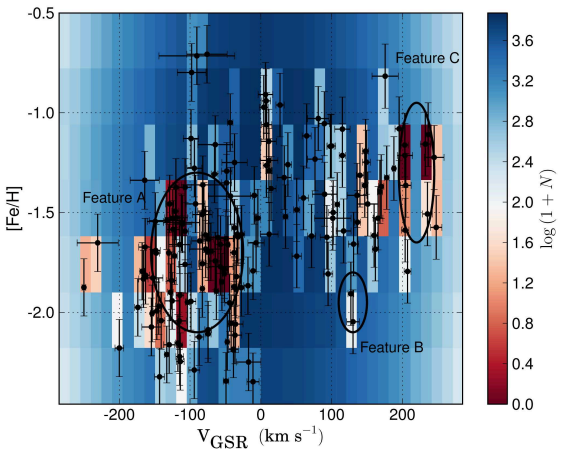

Fig. 4.— Monte-Carlo simulation results illustrating the number of times simulations could reproduce our observed data in the equivalent multi-dimensional bin. Significant features discussed in the text are labelled.

A and C are our most significant structures, and the importance of Feature B becomes more evident through Monte-Carlo simulations. Velocities and metallicities of our K-giants have been binned

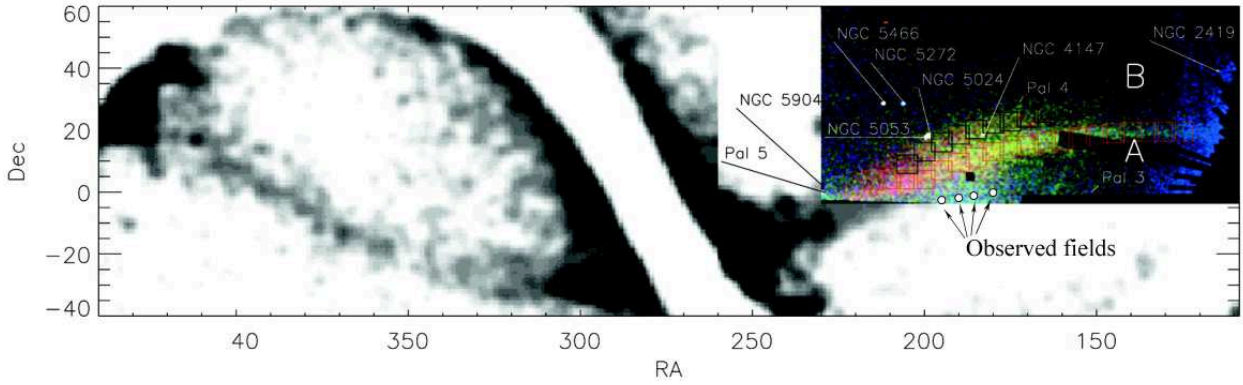

Fig. 5.— Observed fields are outlined upon a panoramic view of the Sgr stream, to demonstrate our field locations in context with the Sagittarius stream. This plot is an adaptation of Figure 2 in Belokurov et al. (2006), which uses the 2MASS M-giant sample of Majewski et al. (2003).

into grid blocks of 15 km s^{-1} and 0.3 dex – roughly twice the error in each dimension. A population of 178 stars were randomly drawn from a simulated halo with canonical kinematics. Metallicities were randomly assigned using the observed Metallicity Distribution Function (MDF) of Ryan & Norris (1991). Each simulated population was binned identically to our observed sample. Simulation grid blocks with counts equal to or exceeding stars in our equivalent observed grid block were noted, and summed after 10,000 simulations. Results from our Monte-Carlo simulations are illustrated in Figure 4. These were consistently significant when the grid was midpoint offset in both dimensions, except for the grid-block centered at $\sim$ 185 km s^{-1} and ~ -1.4 dex, which has consequently been left unlabelled.

Substructure becomes statistically significant when the observed grid blocks are rarely replicated in Monte-Carlo simulations. Specifically, the number of members in Feature A of Figure 3 was never reproduced in some grid bins. This feature is well in excess of the halo and has a wide spread in kinematics. Chou et al. (2007) mapped the Sgr debris across the sky using K/M-giants and found galactocentric velocity signatures between -205 km s^{-1} to -31 km s^{-1} in this region. As such we attribute this wide, significant kinematic peak as the leading arm of the Sagittarius tidal tail. Feature A is discussed in the next section. Another feature where grid blocks were never reproduced in our simulations was Feature C. This feature may also be attributed to Sgr debris and is discussed further in §7.4.

The clump of stars in the velocity bin centered on $V_{GSR} \approx 130$ km s^{-1} and [Fe/H] ≈ -2 was replicated only $\sim$ 1% in 10,000 simulations. We attribute these members to the Virgo Stellar Stream. These members are coincident in spatial position, velocity, and metallicity with previously reported values of the VSS obtained by F turnoff/BHB stars (Newberg et al. 2007) and RR Lyrae stars (Prior et al. 2009b). Feature B is discussed in §7.3.

7.2. Feature A – Sagittarius Debris

The bounds of our observed region are overlaid upon a panoramic projection of the Sagittarius stream, and the "Field of Streams" (Belokurov et al. 2006) in Figure 5. This is a crowded region of globular clusters, substructures and overlapping stellar streams, primarily populated by the Sagittarius Northern arm. Simply from a spatial perspective, we expect the Sgr debris to dominate our data. Although the VOD is present, it is much more diffuse.

7.2.1. Comparing Sagittarius Debris to Dark Halo Models

In order to investigate the spatial coverage and kinematics of our Sagittarius members, we have compared our giants with the constant flattening spheroidal models of LJM05 and the more recent tri-axial model of LM10. The simulated data out-

put from these is readily available online[3], and their released models have the best-fitting parameters for each dark halo shape (prolate, spherical, oblate and tri-axial). These are the only simulations available which make use of an all-sky data set; the 2MASS M-giant sample. We have not considered particles farther than 60 kpc to match realistic observation limitations. For comprehensive details of the simulations the reader is referred to the papers of Law et al. (2005) and Law & Majewski (2010).

The Northern leading arm of Sgr is particularly sensitive both kinematically and spatially to the shape of the Milky Way dark halo (Figure 6). Most models predict the Sgr stream to pass directly through our fields, whereas the prolate model predicts the edge of the stream near this region and no particles directly in our fields. Spatially, the prolate model predicts the Sgr stream to pass much lower in $B_\odot$ than our observed fields. When we extend a rectangle bounded by the edges of our fields (as per the zoomed insets in Figure 6) a mere two particles are predicted. If this prolate halo model is a true representation of the Sgr debris, this does not exclude the potential of finding some Sgr debris in our fields. However, it does imply that if the LJM05 prolate model is an accurate representation of the dark halo then Sgr would not be the dominant population, as we see in our observations.

In comparison the tri-axial, spherical and oblate models predict varying debris from previous peri-centric passages in our fields. A kinematic comparison against our observations is necessary to evaluate model predictions. As the prolate model has only two simulated particles within our extended bounds there is no qualitative kinematic comparison to be made for this model, and as such the prolate model is excluded from further kinematic analysis.

The number of predicted particles observable differs between models. Consequently the kinematics for each model have been represented as a generalised histogram (Figure 7). For consistency all simulation output and observed data has been convolved with a Gaussian kernel of 10 km s^{-1}; the bandwidth used for the previous generalised histogram in Figure 3. Predicted distances and

[3]http://www.astro.virginia.edu/∼srm4n/Sgr/

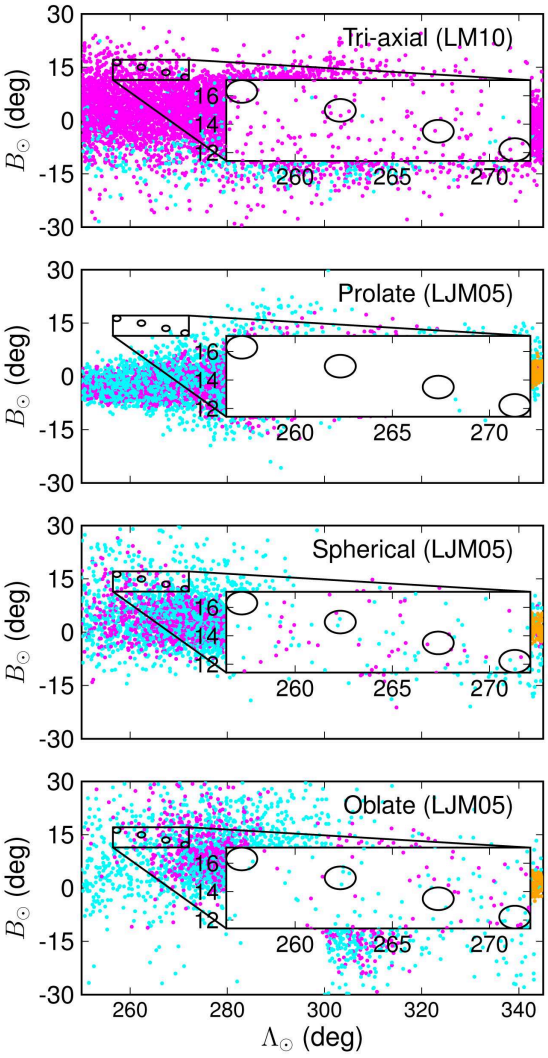

Fig. 6.— Our fields and observed bounds are shown with the simulated particles from multiple N-body simulations by LJM05 and LM10. These particles are distance restricted (up to 60 kpc), and colour-coded by their peri-centric passage following the same convention by Law & Majewski (2010) (orange;most recent passage, magenta; previous passage, cyan; oldest observable passage).

peri-centric ages are shown, demonstrating that debris from multiple passages are predicted along the line of sight. A much tighter velocity sequence is predicted here by the tri-axial model than the constant flattening models. This is because the tri-axial model predicts a pericenter almost pre-

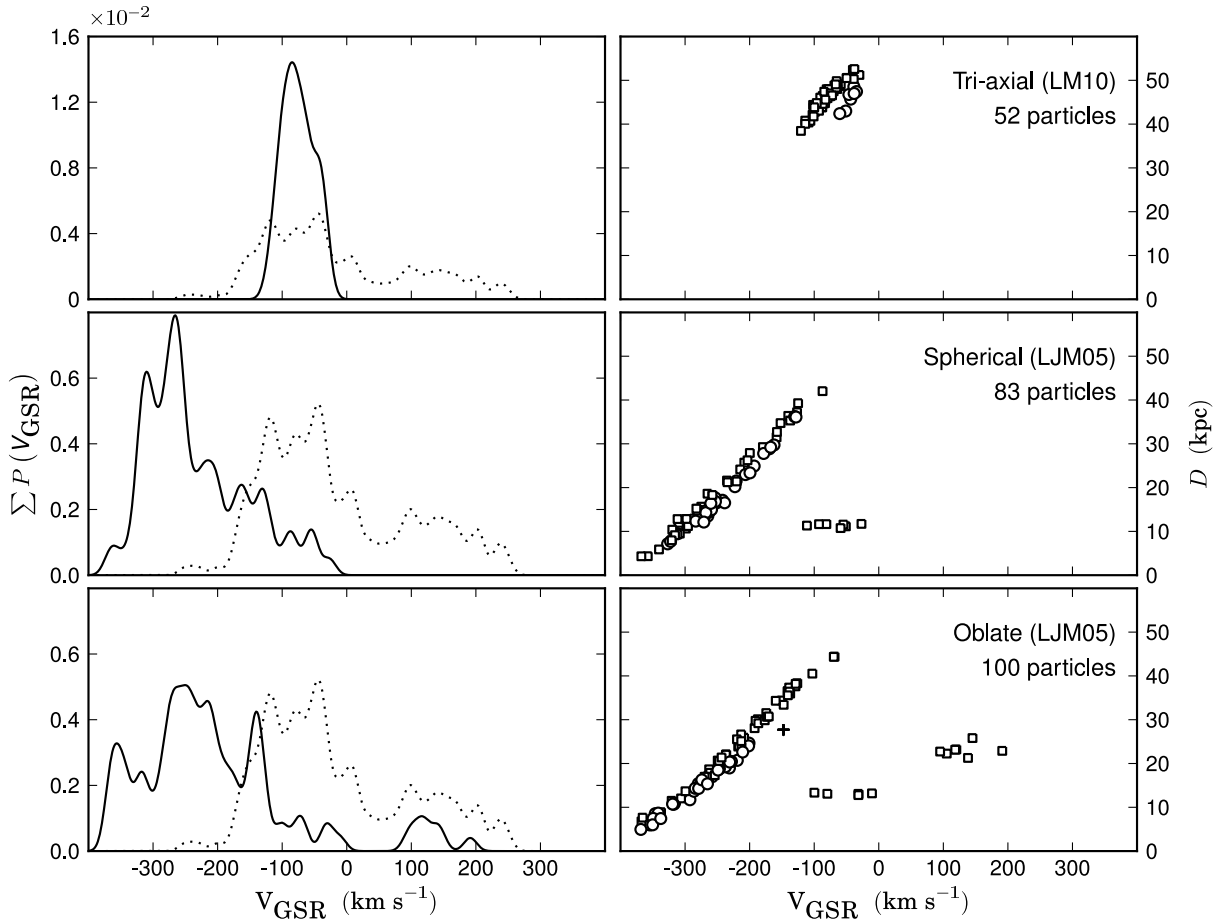

Fig. 7.— A generalised histogram (left) of the galactocentric rest frame velocities in our sample (dotted line) compared to the velocities from the N-body models of LJM05, LM10 of particles within the same spatial coverage and distance range (up to $r_\odot \sim 60$ kpc) of our observed sample (solid line). Heliocentric distances for particles used to generate each velocity histogram are shown on the right. Particles are marked by their recency of passage. A plus (+) denotes debris from the current peri-centric passage by Sgr, circles (∘) mark the previous passage, and squares (□) represent debris from two previous passages. The prolate model from LJM05 is not considered in this plot (see text).

cisely in our observable region, whereas the spherical and oblate models forecast a large wrap along the line of sight, resulting in a wide spread of distances and velocities.

Predicted distances are consistent with what we would expect from our observations. The median luminosities of our giants is $g \sim 17.5$, so for the triaxial model particles at 45 kpc this corresponds to an absolute magnitude of $M_g \sim -0.8$; quite reasonable for a K-giant. Similarly for the spherical and oblate models, typical distances of ~ 25 kpc will yield luminosities of $M_g \sim +0.5$ which is also reasonable.

The spherical and oblate models also predict close-by debris with extremely negative galactocentric velocities. This signature is not represented in our data. Much closer K-giants are less likely to be identified given our luminosity range, although these early K-giants are much more numerous, so this is unlikely to explain our lack of highly negative kinematics. The lowest observed velocity is ~ -250 km s^{-1} and we have only two

observations less than $V_{GSR} < -200$ km s^{-1}. In contrast the spherical/oblate models predict velocities well below $V_{GSR} < -300$ km s^{-1}. These predicted highly negative velocities were also not found in Sgr RR Lyrae observations taken by Prior et al. (2009a). If the dark matter potential is well-represented by either an oblate or spherical halo, then this discrepancy must be reconciled.

The oblate and spherical model also illustrate a similarity signature at $r_{\odot}$ ∼12 kpc, with particle velocities ranging between $-100 < V_{GSR} < 0$ km s^{-1}. This is the edge of a predicted crossing-point between different wraps of the stream, which occurs at ∼ 12 kpc. These particles (and the positive kinematic signature around ∼20 kpc in the oblate model), are relatively minor signatures when compared to the Northern arm feature. If these signatures are present in our observed fields, their relatively low density compared to the northern arm feature would prevent them from appearing as significant.

Although the predicted velocity distribution is narrower than what we observe, the LM10 tri-axial dark halo model best fits our observations. The observed sample broadens most prominently towards more negative galactocentric velocities at ∼ −200 km s^{-1}, still well higher than oblate/spherical predictions. Halo contamination at highly negative velocities is likely to be small. One reconciliation for this tri-axial model/observed kinematic discrepancy may lie in the workings of the tri-axial model itself. Unlike other models considered, the tri-axial model does not reproduce the observed bifurcation in the Sgr stream (Belokurov et al. 2006). Although observationally untested, it is reasonable to suggest a kinematic disruption may consequent from the bifurcation. Such an effect would result in a broader kinematic distribution especially at the stream edges, precisely as seen in our data.

There is further work required through observations and simulations to reconcile kinematic discrepancies. Typical examinations of the leading arm debris usually favour prolate halos and evidence along the trailing arm typically favours oblate halos (Helmi 2004; Martínez-Delgado et al. 2004; Law et al. 2005). Kinematic predictions of the LM10 tri-axial model reasonably match our observations, whereas the prolate model has been excluded as significant debris is not predicted in this edge of the stream. These observations along the Northern leading arm are the first which are not reproducible with the current prolate model of LJM05, contrary to previous groups who have surveyed closer to the leading arm debris.

7.2.2. A Metal-Poor Population Uncovered in Sagittarius Debris

Many groups have found the population of the Sgr core to possess a mean [Fe/H] ∼ −0.5 dex (Cacciari et al. 2002; Bonifacio et al. 2004; Monaco et al. 2005). As the host circles the Milky Way the older, more metal-poor stars are preferentially stripped from the progenitor, creating a metallicity gradient along the stream (Chou et al. 2007; Keller et al. 2010). In this region of the stream, very few Sgr member metallicies have been reported. Vivas et al. (2005) found a mean metallicity of $\langle$[Fe/H]$\rangle = -1.77$ from spectra of 16 RR Lyraes along a nearby region of the Sgr leading arm. Similarly, Prior et al. (2009a) found $\langle$[Fe/H]$\rangle = -1.79 \pm 0.08$ for 21 type *ab* RR Lyrae stars in the region. This is somewhat expected since only the oldest, most metal-poor stars can form RR Lyraes.

Investigating the MDF of the Sgr debris requires an unbiased sample. Generally K-giants are excellent stellar candidates for such investigations as all stars go through this evolutionary phase. If we apply the metallicity gradient found by Keller et al. (2010) to K-giants, we would expect an abundance mean near ∼ − 1.2 dex in this observed region. The metallicity distribution for our entire negative galactocentric sample is shown in Figure 8, and illustrates a notably more metal-poor population than expected. The mean of our distribution is $\langle$[Fe/H]$\rangle = -1.73 \pm 0.33$ dex. If we include only the stars attributed to Feature A (Sgr debris), this value only slightly changes to $\langle$[Fe/H]$\rangle = -1.69 \pm 0.35$. As a comparison, in a sample of metal-rich biased M-giants from the 2MASS data Chou et al. (2007) found a mean metallicity of $\langle$[Fe/H]$\rangle = -0.72$ dex for their best subsample in the Northern leading arm of Sgr.

It is likely that our observed K-giant sample is biased towards more metal-poor members. Given a typical distance of $r_{\odot} \sim 40$ kpc for the Sgr debris in this region (Belokurov et al. 2006), a 12 Gyr old Dartmouth (Dotter et al. 2008) isochrone with a metallicity of [Fe/H] = −1.5 falls directly

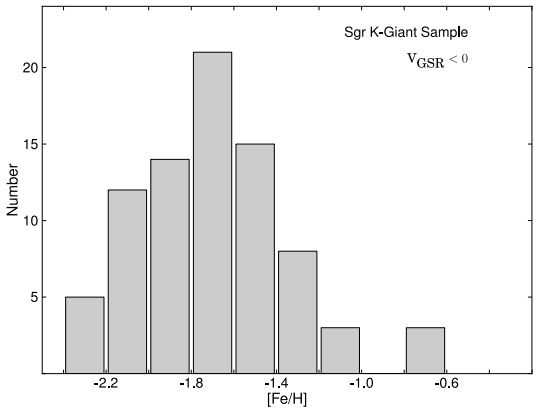

Fig. 8.— Metallicity histograms for K-giant members in our negative galactocentric velocity sample, which is largely populated by Sgr debris from the Northern leading arm.

within our target selection window. The more metal-rich isochrone with [Fe/H] $= -0.5$ does not pass through our selection range. This is consistent with our observed metallicities. Although this does not prohibit the possibility of more metal-rich members within our sample, it implies that our distribution may be biased towards the metal-poor end of the MDF. The tail of our Sgr distribution extends from -0.71 to -2.35 dex.

7.3. Feature B – The Virgo Stellar Stream

One smaller substructure which was distinguished from the general over-density of the VOD is the Virgo Stellar Stream (Duffau et al. 2006). Several RR Lyrae stars were noted with a common velocity of $V_{GSR} = 130$ km s^{-1} (Newberg et al. 2007; Prior et al. 2009b). Prior et al. (2009b) also calculated metallicities of stars with this kinematic signature and found a mean of [Fe/H] $= -1.95 \pm 0.1$ for the VSS, although this is based on RR Lyraes and is metal-poor biased. The RR Lyrae sample from Duffau et al. (2006) found a $\langle [Fe/H] \rangle = -1.86$ with a much larger abundance spread of $\sigma = 0.40$, which was several times the individual $\sigma_{[Fe/H]} = 0.08$ values. This led Duffau et al. (2006) to infer the progenitor of the VSS was likely a dSph galaxy. We also see an abundance spread within this kinematic bin, including some giants with kinematics and metallicities matching those found by Prior et al. (2009b). Monte-Carlo simulations reproduced these few targets a mere $\sim 1\%$ in 10,000 simulations – demonstrating their significance.

High resolution follow-up spectroscopy on these targets and other VSS candidates at higher metallicities in this kinematic range will provide crucial information about the origin of the VSS. Investigating [α/Fe] ratios in these candidates can constrain the mass of the VSS progenitor and discern whether the host was a dSph (Venn et al. 2004; Casetti-Dinescu et al. 2009). Future observations are planned.

7.4. Feature C – Sagittarius debris?

The last significant kinematic substructure in our data is identified as Feature C. There are two peaks identified here at $V_{GSR} = 200$ and 240 km s^{-1}. These features cannot be explained by a smooth halo distribution. Newberg et al. (2007) identified a 4-σ peak at $V_{GSR} = 200$ km s^{-1} in their sample of F turnoff stars on plate $(l, b) = (288°, 62°)$. Our nearest field to their plate (Field B) hosts only one star associated with this peak; most of our these stars are located within our most populated Field D. Prior et al. (2009a) also noted stars in this kinematic range and compiled a list of authors who have also observed such peaks (see Sirko et al. (2004); Duffau et al. (2006); Starkenburg et al. (2009)). Prior et al. (2009a) argue these stars may be associated with trailing debris of Sagittarius, as suggested by models (LJM05, LM10). However there is insufficient evidence to discern strong conclusions.

This substructure has a range of metallicities on our scale. These metallicities were derived with the distance modulus to the VOD/VSS, and may not be exact representations. As such the abundance dispersion we observe is either representative, or these stars have a common metallicity and are dispersed along the line of sight. Unfortunately neither can be positively excluded without further observations. If these peaks are associated with the trailing debris of Sagittarius debris, they are likely to be further away than the VOD. On our scale that would make these stars more metal-rich than shown in Figure 4. However the nearest trailing debris particles predicted from any best-fitting dark halo potential that could explain this kinematic peak occurs at $\sim \Lambda_\odot = 310°$. These observations range in $\Lambda_\odot$ between $256° - 273°$.

Whether this substructure is separate from Sagittarius debris or not remains equivocal.

8. Carbon Stars

In our sample we have identified five carbon stars. With the colour selections to target K-giants, this region also overlaps with where we would expect to find carbon stars (Figure 10). Although these stars were not specifically targeted, their surface densities are so low (≈ 1 per 50 deg^2; Green et al. 1994) that we would not expect them as a substantial contaminant. Although our sky coverage is small ($\sim$12.5 deg^2), the carbon star spatial density is $\sim$ 20x higher than expected. All five carbon stars are recognisable by the presence of distinctive 4737- and 5165 Å Swan C_2 bands.

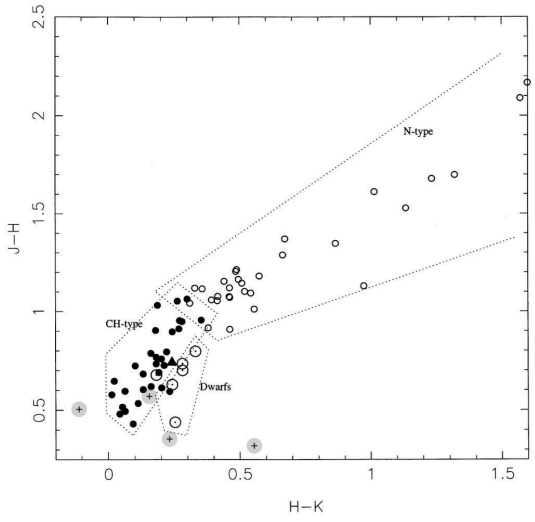

Fig. 9.— J-H and H-K colours for carbon stars recovered by Totten et al. (2000), and those found in this sample. Four of our five carbon stars are represented with plus symbols (+); 2MASS photometry for our faintest carbon star was not available. Carbon stars identified in this work have been shaded for clarity. This plot is an adaptation of Figure 3 in Totten et al. (2000).

Dwarf carbon stars exhibit a spectral signature which mimics that of a typical CH-type giant carbon star, however they have anomalous JHK colours (Green et al. 1992) and unusually high proper motions. These dwarf carbon stars are believed to form in binary systems where material

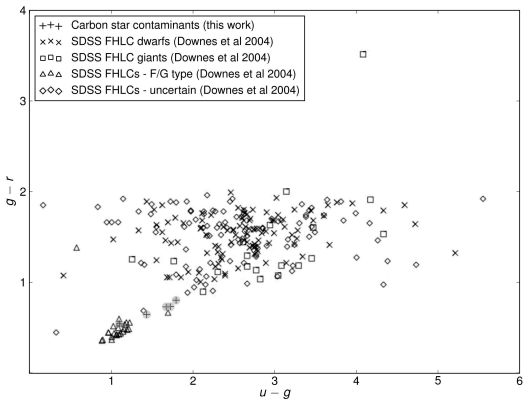

Fig. 10.— Sloan $u - g$ and $g - r$ colours for our carbon stars, and the identified carbon stars and classifications by Downes et al. (2004). Carbon stars identified in this work have been shaded for clarity.

has accreted from a now-invisible companion during its ascent up to the AGB (Dahn et al. 1977). Giant CH-type carbon stars are similar to metal-poor carbon stars found in globular clusters (Harding 1962) and in some dSph galaxies (Demers & Battinelli 2002). The existence of the 4300 Å CH G-band is representative of a CH-type carbon star, and is found in all five of our carbon stars. SDSS photometry for our stars match well with the F/G-type CH carbon stars identified by Downes et al. (2004), as seen in Figure 10. However these targets were not spectroscopically observed in the SDSS follow-up survey SEGUE. Additionally, through comparisons with previous carbon-type star catalogues (Totten & Irwin 1998; Downes et al. 2004; Goswami et al. 2010), the stars tabulated in Table 2 are previously unclassified carbon stars. This is largely because our objects are too faint to have been observed by previous spectroscopic carbon star surveys.

There is 2MASS photometry available for four of these stars. Of those, two stars (SDSS J125410.80-032744.0 and J125416.52-031437.6) exhibit anomalous JHK colours (Figure 9) and significant ($> 3\sigma$) proper motions; characteristics of a dwarf carbon star. A third star also exhibits significant proper motion (SDSS J121740.94-001839.5), however JHK photometry is unavailable. The two remaining stars in our sample have JHK photom-

TABLE 2
PROPERTIES OF CARBON STARS FOUND IN OUR SAMPLE

SDSS Name J+[a]	M_g	u-g	g-r	r-i	i-z	H-K	J-H	$\mu_{\alpha \cos \delta}$[c] (mas yr^{-1})	μ_δ[c] (mas yr^{-1})	V_{GSR} (km s^{-1})
121740.94-001839.5	18.66	1.10	0.54	0.16	0.05	...[b]	...[b]	-3.0 ± 5.4	-18.0 ± 5.4	-71 ± 34
121853.18-004628.4	17.71	1.67	0.73	0.22	0.11	0.24	0.36	-3.7 ± 4.5	-0.5 ± 4.5	$+176 \pm 9$
122053.71-011709.5	17.65	1.79	0.80	0.26	0.13	0.16	0.56	-7.3 ± 4.3	-3.9 ± 4.3	$+31 \pm 11$
125410.80-032744.0	18.59	1.43	0.64	0.22	0.05	0.56	0.32	-21.1 ± 5.0	-7.7 ± 5.0	-41 ± 9
125416.52-031437.6	16.85	1.72	0.73	0.25	0.11	-0.11	0.50	-19.8 ± 4.2	8.7 ± 4.2	$+15 \pm 4$

[a]To keep with convention, positional information has been truncated. Full information available through the SDSS archive.

[b]No *JHK* photometry is available for this object as it is fainter than the 2MASS survey limit.

[c]Proper motions taken from the PPMXL Catalog (Roeser et al. 2010).

etry characteristic of the F/G type CH carbon stars found by Downes et al. (2004) in their faint high-latitude carbon star survey (Figure 10), and do not exhibit significant proper motion - which strongly suggests they are not dwarfs (Green et al. 1994; Deutsch 1994). All identified K-giant stars in our distilled sample had no proper motion detectable above measurement errors. These carbon star kinematics are representative of a typical halo population.

9. Conclusions

We present spectroscopic observations of K-type stars in the crowded 'Field of Streams', where significant substructure is present. Measuring the gravity sensitive Mg I triplet lines in both synthetic and observed spectra, we have demonstrated an excellent dwarf/giant separation criterion. Radial velocities and metallicities of 178 K-giants have been determined. We have recovered kinematic peaks found by other authors, which cannot be explained by a smooth halo distribution. Highly negative velocity signatures match those expected by the Sagittarius stream debris, and we identify a clump of K-giants with metallicities and kinematics which make them highly probable members of the Virgo Stellar Stream.

Stars in this region of the Sagittarius stream are kinematically sensitive to the shape of the Galactic dark halo. As such, we have compared our velocity distribution to the Sgr-Milky Way dark matter models of Law et al. (2005); Law & Majewski (2010). Typically, leading arm debris favour prolate models and trailing arm debris favour oblate models. A prolate dark halo predicts no debris in our observed fields. If the spheroid is prolate and LJM05 presents an accurate representation, we would not expect Sgr debris to dominate our sample (as it does so) even if we were $\Delta B_\odot \sim 10^\circ$ closer to the great circle best-fit. However, Sgr debris is our most significant kinematic structure observed. No single model perfectly represents our data, although we find the more recent tri-axial model (LM10) best represents our observed kinematics. Future tri-axial models with bifurcation treatment are likely to more closely represent these observations.

Observed metallicities for K-giants in this region of the Sgr stream are notably lower than predicted, demonstrating the presence of a metal-poor population in the Sagittarius debris. Although isochrones indicate we are biased towards metal-poor members at these distances, these stars are unequivocally Sagittarius in origin. Metallicity gradients reported suggest a mean of $\langle$[Fe/H]$\rangle \sim -1.2$, whereas our population has $\langle$[Fe/H]$\rangle = -1.73 \pm 0.33$ dex. This suggests either higher abundance gradients along the stream than previously reported, or the Sgr debris has an extremely wide metallically spread. Although biased towards metal-rich members, Chou et al. (2007) find a mean metallicity of $\langle$[Fe/H]$\rangle = -0.72 \pm 0.30$ dex along the leading arm from M-giants. These contrasting observations imply the metallicity distribution function of the debris remains largely unknown. Furthermore, metal-poor K-giants observed here demonstrate that the Sagittarius stream hosts a substantially larger abundance range than previously found.

10. Acknowledgements

SK and GDaC acknowledge the financial support from the Australian Research Council through Discovery Program DP0878137. This publication makes use of data products from the Two Micron All Sky Survey, which is a joint project of the University of Massachusetts and the Infrared Processing and Analysis Center/California Institute of Technology, funded by the National Aeronautics and Space Administration and the National Science Foundation.

REFERENCES

Armandroff, T. E., & Da Costa, G. S. 1991, AJ, 101, 1329

Battaglia, G., Irwin, M., Tolstoy, E., Hill, V., Helmi, A., Letarte, B., & Jablonka, P. 2008, MNRAS, 383, 183

Bell, E. F., et al. 2008, ApJ, 680, 295

Bellazzini, M., Correnti, M., Ferraro, F. R., Monaco, L., & Montegriffo, P. 2006, A&A, 446, L1

Belokurov, V., et al. 2006, ApJ, 642, L137

Bonifacio, P., Sbordone, L., Marconi, G., Pasquini, L., & Hill, V. 2004, A&A, 414, 503

Cacciari, C., Bellazzini, M., & Colucci, S. 2002, in IAU Symposium, Vol. 207, Extragalactic Star Clusters, ed. D. P. Geisler, E. K. Grebel, & D. Minniti, 168–+

Carollo, D., et al. 2007, Nature, 450, 1020

—. 2010, ApJ, 712, 692

Casetti-Dinescu, D. I., Girard, T. M., Majewski, S. R., Vivas, A. K., Wilhelm, R., Carlin, J. L., Beers, T. C., & van Altena, W. F. 2009, ApJ, 701, L29

Castelli, F., & Kurucz, R. L. 2004, ArXiv Astrophysics e-prints

Chou, M., et al. 2007, ApJ, 670, 346

Dahn, C. C., Liebert, J., Kron, R. G., Spinrad, H., & Hintzen, P. M. 1977, ApJ, 216, 757

Demers, S., & Battinelli, P. 2002, AJ, 123, 238

Deutsch, E. W. 1994, PASP, 106, 1134

Dotter, A., Chaboyer, B., Jevremović, D., Kostov, V., Baron, E., & Ferguson, J. W. 2008, ApJS, 178, 89

Downes, R. A., et al. 2004, AJ, 127, 2838

Duffau, S., Zinn, R., Vivas, A. K., Carraro, G., Méndez, R. A., Winnick, R., & Gallart, C. 2006, ApJ, 636, L97

Fellhauer, M., et al. 2006, ApJ, 651, 167

Girardi, L., Grebel, E. K., Odenkirchen, M., & Chiosi, C. 2004, A&A, 422, 205

Goswami, A., Karinkuzhi, D., & Shantikumar, N. S. 2010, MNRAS, 402, 1111

Green, P. J., Margon, B., Anderson, S. F., & Cook, K. H. 1994, ApJ, 434, 319

Green, P. J., Margon, B., Anderson, S. F., & MacConnell, D. J. 1992, ApJ, 400, 659

Harding, G. A. 1962, The Observatory, 82, 205

Harris, W. E. 1996, AJ, 112, 1487

Helmi, A. 2004, ApJ, 610, L97

Helmi, A., & White, S. D. M. 1999, MNRAS, 307, 495

Hinkle, K., Wallace, L., Livingston, W., Ayres, T., Harmer, D., & Valenti, J. 2003, in The Future of Cool-Star Astrophysics: 12th Cambridge Workshop on Cool Stars, Stellar Systems, and the Sun, ed. A. Brown, G. M. Harper, & T. R. Ayres, Vol. 12, 851–856

Ibata, R., Lewis, G. F., Irwin, M., Totten, E., & Quinn, T. 2001, ApJ, 551, 294

Ibata, R. A., Gilmore, G., & Irwin, M. J. 1994, Nature, 370, 194

Ibata, R. A., & Lewis, G. F. 1998, ApJ, 500, 575

Ivezić, Ž., et al. 2000, AJ, 120, 963

Jester, S., et al. 2005, AJ, 130, 873

Johnston, K. V., Law, D. R., & Majewski, S. R. 2005, ApJ, 619, 800

Jurić, M., et al. 2008, ApJ, 673, 864

Keller, S. C. 2010, PASA, 27, 45

Keller, S. C., Murphy, S., Prior, S., Da Costa, G., & Schmidt, B. 2008, ApJ, 678, 851

Keller, S. C., Yong, D., & Da Costa, G. S. 2010, ApJ, 720, 940

Kerr, F. J., & Lynden-Bell, D. 1986, MNRAS, 221, 1023

Kurucz, R. L., & Bell, B. 1995, Atomic Line Data, Kurucz CD-ROM No. 23, (Smithsonian Astrophysical Observatory, Cambridge, MA)

Law, D. R., Johnston, K. V., & Majewski, S. R. 2005, ApJ, 619, 807

Law, D. R., & Majewski, S. R. 2010, ApJ, 714, 229

Law, D. R., Majewski, S. R., & Johnston, K. V. 2009, ApJ, 703, L67

Majewski, S. R., Siegel, M. H., Kunkel, W. E., Reid, I. N., Johnston, K. V., Thompson, I. B., Landolt, A. U., & Palma, C. 1999, AJ, 118, 1709

Majewski, S. R., Skrutskie, M. F., Weinberg, M. D., & Ostheimer, J. C. 2003, ApJ, 599, 1082

Martínez-Delgado, D., Gómez-Flechoso, M. Á., Aparicio, A., & Carrera, R. 2004, ApJ, 601, 242

Mihalas, D., & Binney, J. 1981, Science, 214, 829

Monaco, L., Bellazzini, M., Bonifacio, P., Ferraro, F. R., Marconi, G., Pancino, E., Sbordone, L., & Zaggia, S. 2005, A&A, 441, 141

Newberg, H. J., Yanny, B., Cole, N., Beers, T. C., Re Fiorentin, P., Schneider, D. P., & Wilhelm, R. 2007, ApJ, 668, 221

Newberg, H. J., et al. 2002, ApJ, 569, 245

—. 2003, ApJ, 596, L191

Prior, S. L., Da Costa, G. S., & Keller, S. C. 2009a, ApJ, 704, 1327

Prior, S. L., Da Costa, G. S., Keller, S. C., & Murphy, S. J. 2009b, ApJ, 691, 306

Roeser, S., Demleitner, M., & Schilbach, E. 2010, AJ, 139, 2440

Rutledge, G. A., Hesser, J. E., & Stetson, P. B. 1997, PASP, 109, 907

Ryan, S. G., & Norris, J. E. 1991, AJ, 101, 1865

Schlegel, D. J., Finkbeiner, D. P., & Davis, M. 1998, ApJ, 500, 525

Schoenrich, R., Asplund, M., & Casagrande, L. 2010, ArXiv e-prints

Siegel, M. H., et al. 2007, ApJ, 667, L57

Sirko, E., et al. 2004, AJ, 127, 899

Starkenburg, E., et al. 2009, ApJ, 698, 567

—. 2010, A&A, 513, A34+

Tolstoy, E., Irwin, M. J., Cole, A. A., Pasquini, L., Gilmozzi, R., & Gallagher, J. S. 2001, MNRAS, 327, 918

Totten, E. J., & Irwin, M. J. 1998, MNRAS, 294, 1

Totten, E. J., Irwin, M. J., & Whitelock, P. A. 2000, MNRAS, 314, 630

Tsujimoto, T., Miyamoto, M., & Yoshii, Y. 1998, ApJ, 492, L79+

Venn, K. A., Irwin, M., Shetrone, M. D., Tout, C. A., Hill, V., & Tolstoy, E. 2004, AJ, 128, 1177

Vivas, A. K., Zinn, R., & Gallart, C. 2005, AJ, 129, 189

Vivas, A. K., et al. 2001, ApJ, 554, L33

Watkins, L. L., et al. 2009, MNRAS, 398, 1757

Xue, X.-X., et al. 2010, ArXiv e-prints

York, D. G., et al. 2000, AJ, 120, 1579

Zinn, R., Vivas, A. K., Gallart, C., & Winnick, R. 2004, in Astronomical Society of the Pacific Conference Series, Vol. 327, Satellites and Tidal Streams, ed. F. Prada, D. Martinez Delgado, & T. J. Mahoney, 92–+

This 2-column preprint was prepared with the AAS LaTeX macros v5.2.